NeuroImage 84 (2014) 342–353

Contents lists available at ScienceDirect

NeuroImage

journal homepage: www.elsevier.com/locate/ynimg

Characterization of [^{11}C]Cimbi-36 as an agonist PET radioligand for the 5-HT$_{2A}$ and 5-HT$_{2C}$ receptors in the nonhuman primate brain

Sjoerd J. Finnema [a,*], Vladimir Stepanov [a], Anders Ettrup [b], Ryuji Nakao [a], Nahid Amini [a], Marie Svedberg [a], Charlotte Lehmann [b], Martin Hansen [b], Gitte M. Knudsen [b], Christer Halldin [a]

[a] Karolinska Institutet, Department of Clinical Neuroscience, Center for Psychiatric Research, Stockholm, Sweden
[b] Center for Integrated Molecular Brain Imaging (Cimbi) and Neurobiology Research Unit, Copenhagen University Hospital, Rigshospitalet, Copenhagen, Denmark

ARTICLE INFO

Article history:
Accepted 15 August 2013
Available online 28 August 2013

Keywords:
5-HT$_{2A}$
5-HT$_{2C}$
[^{11}C]Cimbi-36
Agonist
Monkey
Serotonin receptors

ABSTRACT

Only recently the first successful serotonin 2A (5-HT$_{2A}$) receptor agonist PET radioligands have been described, with [^{11}C]Cimbi-36 reported as the most promising in the pig brain so far. Agonist radioligands may target specifically the G protein-coupled state of the receptors and thereby provide a more meaningful assessment of available receptors than antagonist radioligands. In the current study we characterized [^{11}C]Cimbi-36 receptor binding in the primate brain.

On five experimental days, a total of 14 PET measurements were conducted in three female rhesus monkeys. On each day, PET measurements were conducted after intravenous injection of [^{11}C]Cimbi-36 during baseline conditions and after intravenous infusion of the 5-HT$_2$ receptor antagonist ketanserin ($n = 3$) or the 5-HT$_{2C}$ receptor antagonist SB 242084 ($n = 2$). On four of the experimental days an additional baseline PET measurement was conducted after injection of [^{11}C]MDL 100907. All PET measurements were performed for 2 h in a HRRT PET system and arterial blood was obtained for measurement of the [^{11}C]Cimbi-36 input function. Quantification of [^{11}C]Cimbi-36 receptor binding was performed using kinetic and graphical analysis.

After injection of [^{11}C]Cimbi-36 the regional distribution of radioactivity in brain was in accordance with the known 5-HT$_2$ receptor distribution. The two-tissue compartment model was superior for the description of the time–radioactivity curves of all examined brain regions. BP_{ND} values obtained with reference tissue models correlated with corresponding values obtained with kinetic modeling. Administration of ketanserin decreased the binding in all brain regions but did not affect the cerebellar distribution volume. The BP_{ND} of [^{11}C]Cimbi-36 was 56 ± 8% of [^{11}C]MDL 100907 across cortical regions, but higher in other brain regions including choroid plexus. After administration of SB 242084, [^{11}C]Cimbi-36 binding was nearly completely inhibited in the choroid plexus, partly reduced in several subcortical regions (e.g. hippocampus), but not affected in the cortical regions. In conclusion, the receptor binding of [^{11}C]Cimbi-36 can be quantified using kinetic modeling and the cerebellum was found to be a suitable reference region. The difference between [^{11}C]Cimbi-36 and [^{11}C]MDL 100907 binding in the choroid plexus is related to 5-HT$_{2C}$ receptor binding of [^{11}C]Cimbi-36. [^{11}C]Cimbi-36 is the first agonist radioligand suitable for examination of 5-HT$_{2A}$ receptors in the cortical regions and of 5-HT$_{2C}$ receptors in the choroid plexus of the primate brain.

Introduction

The serotonin (5-hydroxytryptamine, 5-HT) system plays an important role in normal physiological processes, such as mood, sleep and appetite. Dysfunction of the 5-HT system is thought to be the key in the pathophysiology of several brain disorders, such as depression. Thus far, fourteen mammalian receptor subtypes have been characterized and assigned to seven receptor families, 5-HT$_{1-7}$ (Hoyer and Martin, 1997). Evaluation of these receptors in the living human brain is possible using positron emission tomography (PET), with suitable radioligands being available for 5-HT$_{1A}$, 5-HT$_{1B}$, 5-HT$_{2A}$, 5-HT$_4$ and 5-HT$_6$ receptors (Parker et al., 2012; Paterson et al., 2013).

PET studies examining 5-HT$_{2A}$ receptors have been conducted to evaluate the role of 5-HT$_{2A}$ receptors in physiology (Erritzoe et al., 2009) and neuropsychiatric disorders (Adams et al., 2005; Haugbol et al., 2007). A limitation of the available 5-HT$_{2A}$ receptor PET radioligands, e.g. [^{18}F]altanserin (Biver et al., 1994; Lemaire et al., 1991) or [^{11}C]MDL 100907 (Ito et al., 1998; Lundkvist et al., 1996), is that they are antagonists. Classical receptor binding assay studies have demonstrated that 5-HT$_{2A}$ receptors exist in two affinity states for agonists (Fitzgerald et al., 1999; Lopez-Gimenez et al., 2001c; Song et al., 2005), similar as for other G protein-coupled receptors. The receptor affinity states are considered interconvertible, with the high-affinity state thought to represent the G

* Corresponding author at: Karolinska Institutet, Department of Clinical Neuroscience, Center for Psychiatric Research, Karolinska University Hospital, Building R5:02, SE-17176 Stockholm, Sweden. Fax: +46 8 51771753.
E-mail address: sjoerd.finnema@ki.se (S.J. Finnema).

1053-8119/$ – see front matter © 2013 Elsevier Inc. All rights reserved.
http://dx.doi.org/10.1016/j.neuroimage.2013.08.035

protein-coupled state of the receptor (Kent et al., 1980). Agonist radioligands have thus potential for selective imaging of receptors in the high-affinity state and may provide additional value to antagonist radioligands by making corresponding PET imaging more functionally relevant.

Another possible advantage of agonistic PET radioligands is an enhanced sensitivity to endogenous neurotransmitter concentrations. Indeed, dopamine D_2 and D_3 receptor agonist radioligands have been found to have an enhanced sensitivity to endogenous dopamine concentrations than antagonist radioligands (Ginovart et al., 2006; Narendran et al., 2004, 2010; Seneca et al., 2006; Shotbolt et al., 2012). Since 5-HT_{2A} receptor antagonist PET radioligands have no or very limited sensitivity to changes in endogenous serotonin concentrations (Hirani et al., 2003; Pinborg et al., 2004; Quednow et al., 2012; Staley et al., 2001), an agonist radioligand may provide additional value to the available 5-HT_{2A} receptor antagonist radioligands.

Only recently, the first agonist radioligands for the 5-HT_{2A} receptor were described, with [^{11}C]Cimbi-36 reported as the most promising so far (Ettrup et al., 2010, 2011). Cimbi-36 has high affinity to the rat 5-HT_{2A} receptor expressed in a NIH-3T3 cell line (K_i (nM): 0.5 nM) (Ettrup et al., 2011). Evaluation of Cimbi-36 in the Psychoactive Drug Screening Program (PDSP) confirmed the high affinity to 5-HT_2 receptors (K_i (nM): 5-HT_{2A} = 0.5–0.8; 5-HT_{2B} = 0.5; 5-HT_{2C} = 1.7) and demonstrated a high selectivity over other targets (>120-fold) (Ettrup et al., 2011). The intrinsic activity of Cimbi-36 was 87% of that of 10 μM serotonin to 5-HT_{2A} receptors using an in vitro phosphatidylinositol (PI) hydrolysis assay (Ettrup et al., 2011) and the agonistic properties have been confirmed by in vivo head-twitch response (HTR) studies (Ettrup et al., 2013). After injection of [^{11}C]Cimbi-36 in a pig, the radioactivity accumulated predominantly in the neocortex which is consistent with the known distribution of 5-HT_{2A} receptors. The nondisplaceable binding potential (BP_{ND}) estimate for the neocortex was promising (0.82), and likely an underestimate, as the reference region, cerebellum, contains 5-HT_{2A} receptors in the pig brain (Hansen et al., 2013). Specific [^{11}C]Cimbi-36 binding to 5-HT_{2A} receptors was confirmed by administration of the 5-HT_2 receptor antagonist ketanserin (Ettrup et al., 2011). Thus [^{11}C]Cimbi-36 can be considered a promising radioligand for evaluation of 5-HT_{2A} receptor agonist binding in the living primate brain.

In the current study, we for the first time quantified and characterized the binding of [^{11}C]Cimbi-36 in the nonhuman primate brain. PET measurements were performed after i.v. injection of [^{11}C]Cimbi-36 during baseline conditions (n = 5) and after pretreatment with the 5-HT_2 receptor antagonist ketanserin (n = 3) or the 5-HT_{2C} receptor antagonist SB 242084 (n = 2). On four of the five experimental days an additional baseline PET measurement was conducted after injection of the 5-HT_{2A} receptor antagonist [^{11}C]MDL 100907, to allow for comparison of regional binding with [^{11}C]Cimbi-36. Arterial blood was obtained for measurement of the [^{11}C]Cimbi-36 input function and to allow for quantification of [^{11}C]Cimbi-36 receptor binding using kinetic and Logan graphical analysis (GA).

Materials and methods

Preparation of [^{11}C]MDL 100907 and [^{11}C]Cimbi-36

[^{11}C]MDL 100907 was prepared using previously described procedures (Lundkvist et al., 1996). The radiosynthesis of [^{11}C]Cimbi-36 was performed in a similar manner as described earlier (Ettrup et al., 2011). The standard Cimbi-36 (2-(4-bromo-2,5-dimethoxyphenyl)-*N*-(2-methoxybenzyl)ethanamine) and the corresponding *O*-desmethyl-precursor (Cimbi-37) were prepared at the Department of Drug Design and Pharmacology, Faculty of Health and Medical Sciences, University of Copenhagen. In short, [^{11}C]Cimbi-36 was radiolabeled using [^{11}C]methyl triflate ([^{11}C]CH_3OTf), which was prepared from in-target produced [^{11}C]methane via [^{11}C]methyl iodide (Andersson et al., 2009). [^{11}C]CH_3OTf was trapped at room temperature in a reaction vessel containing the precursor Cimbi-37 (0.4–0.6 mg), acetonitrile (300 μL), acetone (300 μL) and aqueous sodium hydroxide (3 M) (2–3 μL). After approximately 60 s, 1000 μL of trifluoroacetic acid/acetonitrile 1/2 *v*/*v* mixture was added to the reaction vessel and the mixture was heated to 80 °C for 5 min. After cooling to room temperature, the reaction mixture was neutralized with aqueous sodium hydroxide (3 M) (1000 μL) and injected into the semi-preparative high-performance liquid chromatography (HPLC) system for purification. The HPLC system contained a C-18 μ-Bondapak column (300 mm × 7.8 mm, 10 μm; Waters, Milford, MA, USA) and a Knauer ultraviolet (UV) absorbance detector (λ = 254 nm; VWR International, Stockholm, Sweden) in series with a Geiger–Müller tube (Carrol–Ramsey, Berkeley, CA, USA) for radioactivity detection. For purification, a mobile phase system of acetonitrile and aqueous ammonium formate (0.1 M) 46/54 *v*/*v* was used at 6 mL/min. The desired fraction was collected into a vial containing 60 mL of water and 70–100 mg of sodium ascorbate. The resulting solution was pushed through Oasis® HLB cartridge (Waters) previously conditioned by rinsing it with 10 mL ethanol and 10 mL water. After the trapping of the product, the cartridge was rinsed with 8 mL distilled water, and the product was then eluted with 1.0 mL 99.6% ethanol and collected in a sterile receiving vial prefilled with 10 mL sterile physiological phosphate buffer solution (PBS) (pH = 7.4). The solution was finally filtered through a Millex-GV filter unit (0.22 μm) (Millipore, Billerica, MA, USA).

The radiochemical purity and the identity of the final radioactive product were determined using an analytical HPLC system (Hitachi, Tokyo, Japan) containing an UV absorption detector (λ = 254 nm) and a β-flow radiodetector (Beckman Instruments, Fullerton, CA, USA) in series. The chromatography system used was an ACE 5 C-18 column (250 mm × 4.6 mm, 5 μm; Advanced Chromatography Technologies, Aberdeen, Scotland) eluted (2 mL/min) with a mobile phase system of acetonitrile and aqueous ammonium formate (0.1 M) 40/60 *v*/*v*. The identity of the radioactive product of the final formulated products was evaluated by co-injection with unlabelled reference and was further confirmed using LC-MS/MS (Andersson et al., 2010). The specific radioactivity of the final product was determined using an analytical HPLC system (λ = 214 nm) containing an ACE 5 C18-HL column (250 mm × 4.6 mm, 5 μm; Advanced Chromatography Technologies) eluted (2 mL/min) with a mobile phase system of acetonitrile and aqueous phosphoric acid (50 mM) 30/70 *v*/*v*.

Nonhuman primates

The study was approved by the Animal Research Ethical Committee of the Northern Stockholm region (Dnr N386/09 and N452/11) and was performed according to local (Dnr 4820/06-600) and international guidelines (Garber et al., 2011). Three female rhesus monkeys (*Macaca mulatta*), weighing 7–11 kg, were included in the study. The monkeys are housed in the Astrid Fagraeus Laboratory, Comparative Medicine, Karolinska Institutet, Solna, Sweden.

PET system

PET measurements were conducted using the High Resolution Research Tomograph system (Siemens Molecular Imaging, Knoxville, TN, USA). A six minute transmission scan using a single ^{137}Cs source was obtained immediately before the radioligand injection. List-mode data were acquired for 123 min. PET images were reconstructed with a series of frames of increasing duration (9 × 10 s, 2 × 15 s, 3 × 20 s, 4 × 30 s, 4 × 60 s, 4 × 180 s, 17 × 360 s) using the ordinary Poisson 3-dimensional ordered-subset expectation maximization (OP-3D-OSEM) algorithm, with 10 iterations and 16 subsets, including modeling of the point spread function, after correction for attenuation, random and scatter. The in-plane resolution of the reconstructed images is approximately 1.5 mm (Varrone et al., 2009).

PET experimental procedures

Anesthesia of the monkeys was induced by intramuscular injection of ketamine hydrochloride (~10 mg/kg, Ketaminol vet.; Intervet, Sollentuna, Sweden) and maintained by the administration of a mixture of sevoflurane (2%–8%, sevoflurane®; Abbot Scandinavia AB, Solna, Sweden), oxygen, and medical air after endotracheal intubation. The head was immobilized with a fixation device (Karlsson et al., 1993). Body temperature was maintained by a Bair Hugger device (model 505; Arizant Health Care, Eden Prairie, MN, USA) and monitored by an oral thermometer. Electrocardiogram, heart rate, respiratory rate, oxygen saturation, and arterial blood pressure were continuously monitored throughout the experiments. The radioligand was intravenously administered in a sural vein of the monkey by a bolus administration of radioligand (~150 MBq in 4 mL) over ~5 s, followed by a 2 mL saline flush. A cannula was inserted in the femoral artery or an artery of the lower limb, and arterial blood was collected continuously for 3 min using an automated blood sampling system (ABSS) (Allogg, Mariefred, Sweden) at a speed of 3.0 mL/min. Blood samples (1.0–3.0 mL) were drawn at 0.5, 1.0, 1.5, 2.0, 3.0, 6.0 and 8.0 min for blood and plasma radioactivity and at 2.5, 5.0, 10, 20, 40, 60, 90 and 120 min for metabolite correction. One blood sample (1.5–2.0 mL) was taken before each radioligand injection for determination of protein binding.

Study design

A total of 14 PET measurements were performed on five experimental days. On four experimental days three PET measurements were performed and on one experimental day two PET measurements were performed. During the experimental days, the PET measurements were conducted two and an half hours apart.

To evaluate the quantification of the receptor binding of [^{11}C]Cimbi-36, on each day a baseline PET measurement was obtained after injection of [^{11}C]Cimbi-36 and included arterial blood sampling.

To allow for comparison of [^{11}C]Cimbi-36 receptor binding with [^{11}C]MDL 100907, on four of the experimental days a baseline PET measurement was obtained after injection of [^{11}C]MDL 100907. The order of the baseline measurements of [^{11}C]Cimbi-36 and [^{11}C]MDL 100907 was counter balanced. During the [^{11}C]MDL 100907 PET measurements only one blood sample was collected for determination of protein binding.

The final PET measurement on the experimental days consisted of a [^{11}C]Cimbi-36 injection after pretreatment of the monkey with the 5-HT_2 receptors antagonist ketanserin ($n = 3$) (Leysen et al., 1981) or the 5-HT_{2C} receptor antagonist SB 242084 ($n = 2$) (Bromidge et al., 1997; Kennett et al., 1997) and included arterial blood sampling. Ketanserin was infused i.v. over 30 min, starting 45 min before the [^{11}C]Cimbi-36 injection. The examined dose of ketanserin was based on previous PET studies (Lundkvist et al., 1996) and was on one day 1.5 mg/kg (NHP1) and on the other two days 0.75 mg/kg. Ketanserin ((+)-tartrate salt; Sigma-Aldrich, Schnelldorf, Germany) was formulated in a mixture of ethanol (9%, *v*/*v*), propylene glycol (21%, *v*/*v*) and PBS (70%, *v*/*v*) and the reported doses refer to the salt. SB 242084 was infused i.v. over 15 min, starting 30 min before the [^{11}C]Cimbi-36 injection. The examined dose of SB 242084 was based on literature (Manvich et al., 2012a,b) and was 1.0 mg/kg. SB 242084 (dihydrochloride salt; Tocris, Bristol, U.K.) was formulated in a mixture of ethanol (10%, *v*/*v*), PEG 400 (20%, *v*/*v*) and 25% (w/v) captisol® (70%, *v*/*v*) and the reported dose refers to the salt.

Image analysis

Volumes of interest (VOIs) were delineated on MR images, guided by an atlas of a rhesus monkey brain (Saleem and Logothesis, 2007). An average PET image (mean of the time frames corresponding to 0–57 min) was automatically coregistered to the MR image using the Fusion module in the software PMOD (version 3.308; PMOD Technologies, Zurich, Switzerland). VOIs were defined for the amygdala, caudate nucleus, cerebellum, choroid plexus, cingulate cortex, dorsolateral prefrontal cortex, hippocampus, insular cortex, midbrain, occipital cortex, orbital prefrontal cortex, parietal cortex, putamen, temporal cortex, thalamus, ventral striatum and whole brain. The VOI for the cerebellum included only the cerebellar hemispheres. The striatum was defined as the volume weighted mean of the caudate nucleus, putamen and ventral striatum. The cortical regions VOI represents the mean of all evaluated cortices. The VOI for the choroid plexus was defined around the radioactivity in the fourth ventricle using fused PET/MR images displayed in the transaxial projection.

Decay-corrected time–activity curves for all regions were plotted over time and radioactivity concentrations were expressed as standardized uptake value (SUV) and calculated as radioactivity concentration [kBq/cm^3] / (radioactivity injected [MBq] / body weight [kg]). The cerebellum was considered the reference region.

Radiometabolite analysis

A reversed-phase HPLC method was used to determine the percentages of radioactivity in monkey plasma that correspond to unchanged radioligand and radiometabolites during the course of the PET measurements. The plasma (0.5–1.5 mL), obtained after centrifugation of blood at 2000 *g* for 2–4 min, was mixed with 1.4 times volume of acetonitrile. After stirring with a vortex mixer, the sample was centrifuged at 2000 *g* for 2–4 min and 2 mL of water was added to the supernatant plasma-acetonitrile mixture, which was then injected to a radio-HPLC system. The blood (1.0–3.0 mL) and plasma (0.5–1.5 mL) were counted in a NaI well-counter. The radioactivity of protein precipitate fraction was also measured to quantify the recovery after precipitation with acetonitrile. The radio-HPLC system used in the plasma experiments consisted of an interface module (D-7000; Hitachi), a pump (L-7100; Hitachi), an injector (7125, 5.0 mL loop; Rheodyne, Cotati, CA, USA) equipped with a C18 μ-Bondapak column (300 × 7.8 mm, 10 mm; waters), and an UV absorbance detector (L-7400, λ = 280 nm; Hitachi) in series with a dual bismuth germanium oxide coincidence radiation detector (S-2493Z; Oyokoken, Fussa, Japan) equipped with a 550 mL flow cell. Acetonitrile (A) and ammonium formate (100 mM) (B) were used as the mobile phase at 6.0 mL/min, according to the following program: 0–8 min (A/B), 40/60 → 75/25 *v*/*v*; 8–10 min (A/B), 75/25 *v*/*v*; and 10–12 min (A/B), 40/60 *v*/*v*. Peaks for radioactive compounds eluting from the column were integrated and their areas were expressed as a percentage of the sum of the areas of all detected radioactive compounds (decay-corrected to the time of injection on the HPLC).

Measurement of protein binding

The free fraction, f_p, of [^{11}C]Cimbi-36 and [^{11}C]MDL 100907 in plasma was estimated using an ultrafiltration method. Monkey plasma (500 μL), or PBS solution (500 μL) as a control, was mixed with radioligand formulation (50 μL, ~1 MBq) and incubated at room temperature for 10 min. After the incubation, 200 μL portions of the incubation mixtures were pipetted into ultrafiltration tubes (Centrifree YM-30, molecular weight cutoff, 30,000; Millipore) and centrifuged at 1500 *g* for 15 min. Equal aliquots (20 μL) of the ultrafiltrate (C_{free}) and of the plasma (C_{total}) were counted for their ^{11}C radioactivity with a NaI well-counter. Each determination was performed in duplicate. The free fraction of [^{11}C]Cimbi-36 was calculated as $f_p = C_{free} / C_{total}$, and the results were corrected for the membrane binding measured with the control samples.

Quantification

Kinetic analysis was performed both with a 1-tissue-compartment model (1TCM) and a 2-tissue compartment model (2TCM). GA was performed with the Logan plot (Logan et al., 1990). The time of

equilibrium (t*) of 27 min was used for measuring the slope of the linear part of the Logan plot. The outcome measures were total distribution volume (V_T) (5-HT_2 receptor-rich regions) and nondisplaceable distribution volume (V_{ND}) (cerebellum) (Innis et al., 2007). The binding potentials (*BP*), relative to the concentration of nondisplaceable radioligand in tissue (BP_{ND}) and relative to the free concentration of radioligand in plasma (BP_F), were estimated using the cerebellum as a reference region. BP_{ND} values were also estimated using the noninvasive GA (NIGA) method (Logan et al., 1996) and the simplified reference tissue model (SRTM) (Lammertsma and Hume, 1996). Kinetic and GAs were performed using PMOD module kinetic. Parametric V_T maps were generated with GA using PMOD module PXMod.

The total plasma concentration of [^{11}C]Cimbi-36 was used as an input function, and the radioactivity concentration in blood was used for blood volume (*vB*) correction. The time delay between the arrival of the tracer at the ABSS detector and in the brain was estimated by a preliminary fitting of the whole-brain time radioactivity curve with a 2TCM. The Levenberg–Marquardt algorithm for the iterative minimization of the cost function was used for the nonlinear least squares fitting. A constant weighing factor was applied with a scale factor of 0.05. The Akaike information criterion (Akaike, 1974) and F statistics of the sum of squared residuals (Carson, 1986) were used to compare the fitting of the compartment model analyses. The identifiability of parameters was expressed by the percentage of the coefficient of variation (%COV).

In vitro autoradiography

Sagittal cynomolgus monkey (*Macaca fascicularis*) sections at 20 μm or transaxial human whole hemisphere sections at 100 μm were thawed and pre-incubated in binding buffer (Tris HCl 50 mM pH 7.4, incl. 120 mM NaCl, 5 mM KCl, 2 mM $CaCl_2$ and 1 mM $MgCl_2$). Monkey sections were incubated in [^{3}H]Cimbi-36 at 3, 1, 0.3, 0.1 and 0.03 nM in binding buffer for 120 min. Human sections were incubated at 0.5 nM [^{3}H]MDL 100907 or [^{3}H]Cimbi-36 in binding buffer for 60 and 120 min, respectively. In duplicate sets of containers nonspecific binding was determined by 10 μM ketanserin.

Following incubation, slides were washed for 5 min ([^{3}H]MDL 100907) or 10 min ([^{3}H]Cimbi-36), twice in ice-cold Tris HCl 50 mM pH 7.4, followed by a brief wash in distilled water. The slides were dried and exposed to phosphor imaging plates (BAS-TR2025; Fujifilm, Tokyo, Japan). Micro scale standards (American Radiolabeled Chemicals, St. Louis, MO, USA) were exposed together with the sections for calibration and quantification of the binding density. The phosphor imaging plates were scanned and the resulting images were processed in a phosphor imager (BAS-5000; Fujifilm). Analysis was performed using Multi Gauge 3.2 phosphorimager software (Fujifilm). Specific binding, which is an indication of receptor density, were calculated by subtracting the level of nonspecific binding from the total binding for each section.

Results

Preparation of [^{11}C]Cimbi-36 and [^{11}C]MDL 100907

The radiochemical purity of [^{11}C]Cimbi-36 was over 97% and the average specific radioactivity obtained at time of injection of [^{11}C]Cimbi-36 was 342 GBq/μmol (range: 77–549 GBq/μmol, $n = 10$), corresponding to a mean injected mass of 0.25 μg (range: 0.11–0.74 μg, $n = 10$) in the monkey. [^{11}C]Cimbi-36 was stable in the PBS formulation for up to at least 2 h.

The radiochemical purity of [^{11}C]MDL 100907 was over 99% and the average specific radioactivity obtained at time of injection was 550 GBq/μmol (range: 443–716 GBq/μmol, $n = 4$), corresponding to a mean injected mass of 0.11 μg (range: 0.08–0.13 μg, $n = 4$) in the monkey.

Radiometabolite analysis and protein binding

A representative HPLC radiochromatogram, obtained at 40 min after injection of [^{11}C]Cimbi-36, is displayed in Fig. 1A. After injection of [^{11}C]Cimbi-36 4–6 radiometabolite fractions could be measured during the time course of the PET measurement. The two main radiometabolite fractions had a retention time (tR) of 2.3 ([^{11}C]M1) and 3.5 ([^{11}C]M2) minutes, respectively, and eluted earlier than [^{11}C]Cimbi-36 (8.8 min). [^{11}C]Cimbi-36 was rapidly metabolized, accounting for 22 ± 3% of the plasma radioactivity at 20 min and for 10 ± 1% at 120 min after injection (Fig. 1B). The f_p was 0.05 ± 0.01 for [^{11}C]Cimbi-36 and 0.5 ± 0.1 for [^{11}C]MDL 100907 during baseline conditions.

Quantification of [^{11}C]Cimbi-36 receptor binding

The radioactivity in plasma reached a peak shortly after injection of [^{11}C]Cimbi-36 (Fig. 1C). The plasma radioactivity decreased rapidly during the first 3 min and continued to decline slowly throughout the PET measurement.

After injection of [^{11}C]Cimbi-36, the whole brain radioactivity concentration rapidly increased and peaked after 10–20 min, with a maximum radioactivity concentration ranging from 1.7 to 2.6 SUV. The highest radioactivity concentrations were observed in the cortical regions and choroid plexus (Figs. 1D and 2); more moderate concentrations were measured in the hippocampus and amygdala; whereas the concentrations were lowest in the midbrain and cerebellum.

The first step in the kinetic analysis included the estimation of the delay and the blood volume. The estimated delay was 7 ± 3 s and the estimated *vB* was 0.06 ± 0.02 across brain regions ($n = 15$) and 0.09 ± 0.02 in the choroid plexus.

Fitting of the 1TCM and the 2TCM to the regional time radioactivity curves (Fig. 1D) yielded rate constants, of which values for the cortical regions, the choroid plexus and the cerebellum are presented in Table 1. The time radioactivity curves from the cortical regions, subcortical regions, choroid plexus and cerebellum were best described with the 2TCM (F test, $P < 0.01$). The estimated K_1 was 0.21 ± 0.03 in the choroid plexus which was higher than in other brain regions, e.g. cortical regions 0.14 ± 0.03. The 2TCM provided reliable V_T estimates, except for the choroid plexus in one measurement, which was then excluded from further model comparisons. The 2TCM provided estimated V_T and V_{ND} values were 10% higher than with the 1TCM (Table 2). V_T values obtained with the 1TCM were closely correlated with the 2TCM (Pearson $r = 0.9755$, $P < 0.0001$) (Fig. 3A).

In the GA with arterial input a linear phase was observed from 27 min for all regions. The GA provided estimated V_T values were 9% lower than the 2TCM (Table 2). V_T values obtained with the GA were correlated with the 2TCM (Pearson $r = 0.9711$, $P < 0.0001$) and 1TCM (Pearson $r = 0.9866$, $P < 0.0001$) (Figs. 3B, C). BP_{ND} values obtained with the GA method were in close correlation with the BP_{ND} values estimated with the 2TCM (Pearson $r = 0.9468$, $P < 0.0001$) (Table 2 and Fig. 3D).

In the next step, the cerebellum was used as a reference region in the NIGA and in the SRTM. BP_{ND} values obtained with the NIGA (Pearson $r = 0.9505$, $P < 0.0001$) and the SRTM (Pearson $r = 0.9439$, $P < 0.0001$) were in close correlation with the BP_{ND} values estimated with the 2TCM (Figs. 3E, F) although both reference tissue models underestimated BP_{ND} values with an average of 21 and 23%, respectively (Table 2).

To assess the time stability of the estimated V_T and BP_{ND} values, the effect of the duration of the PET measurement on the parameters was evaluated. The time radioactivity curves for the cerebellum and cortical regions were analyzed using the 2TCM, GA and SRTM using different PET measurement durations ranging from 123 to 63 min. All V_T and BP_{ND} values were properly estimated using 123 min of PET duration. (Supplementary Fig. 1).

Blocking studies and comparison with [^{11}C]MDL 100907

Administration of the 5-HT$_2$ receptor antagonist ketanserin decreased [^{11}C]Cimbi-36 binding in all brain regions, except in the cerebellum (Fig. 4A). The mean reduction in [^{11}C]Cimbi-36 binding in the BP_{ND} for the cortical regions was 85 ± 1% (Table 3). The corresponding Lassen plots (Fig. 4B) yielded slopes indicating a 5-HT$_2$ receptor occupancy of 91 ± 2%. The V_{ND} values as estimated with the 2TCM cerebellar V_T were 4.6 ± 0.8 cm^3/mL without and 4.6 ± 0.9 cm^3/mL after ketanserin administration, in good correspondence with the mean x-axis intercept (V_{ND}) in the Lassen plots being 5.4 ± 1.3 cm^3/mL. Administration of ketanserin did not affect the f_p significantly (0.06 ± 0.01), in comparison to baseline conditions.

The binding of [^{11}C]Cimbi-36 was lower than with [^{11}C]MDL-100907, with [^{11}C]Cimbi-36 BP_{ND} estimates (SRTM) in the cortical regions being 56 ± 8% of [^{11}C]MDL-100907. More detailed comparison indicated also regional differences in radioligand binding. After [^{11}C]Cimbi-36 injection there was high binding in the choroid plexus, while for [^{11}C]MDL-100907 the binding in choroid plexus was approaching that in the cerebellum (Figs. 5A, B). The relative binding of [^{11}C]Cimbi-36 over [^{11}C]MDL-100907 was in the midbrain, hippocampus, amygdala and thalamus higher than in the cortical regions (Fig. 6).

Administration of the 5-HT$_{2C}$ receptor antagonist SB 242084 increased [^{11}C]Cimbi-36 uptake into the brain, yielding a 101% increase in the V_T of the cortical regions (Table 4). This increase was related to an SB 242084-induced increase in the f_p (0.10 vs. 0.05 ± 0.01 during baseline conditions). The reduction in specific [^{11}C]Cimbi-36 binding approached complete inhibition in the choroid plexus, but was more heterogeneous across other brain regions (Figs. 2, 5 and 6, Table 4). The [^{11}C]Cimbi-36 binding in the cortical regions was not affected, while binding in the midbrain, hippocampus, amygdala and thalamus was reduced to different extents. The brain regions in which SB 242084-induced inhibition was observed, corresponded with the brain regions with relative high binding of [^{11}C]Cimbi-36 over [^{11}C]MDL-100907 (Fig. 7). After administration of SB 242084 the relative binding of [^{11}C]Cimbi-36 over [^{11}C]MDL-100907 was more similar (ratio of 0.5–0.8) across brain regions and on the same level as for the cortical regions (0.6), except for in the choroid plexus and midbrain.

In vitro autoradiography

[^{3}H]Cimbi-36 bound in a saturable manner in the monkey brain, with an apparent K_D value of 1.3 nM across examined brain regions (Supplementary Fig. 2). The density of the 5-HT$_{2A}$ receptors in the human brain, as measured by [^{3}H]MDL 100907 and [^{3}H]Cimbi-36, are shown in Fig. 7. The highest densities of specific [^{3}H]MDL 100907 binding were found in the hippocampus (17.1 fmol/mg tissue wet weight) and frontal cortex (6.4 fmol/mg) with lower binding in the cerebellum (0.1 fmol/mg) (Fig. 7A). The [^{3}H]MDL 100907 binding was almost blocked completely by the addition of 10 μM ketanserin (Fig. 7B). High density of [^{3}H]Cimbi-36 specific binding was found in choroid plexus (Fig. 7C), resembling that shown in vivo by PET (Fig. 2). [^{3}H]Cimbi-36 specific binding in the hippocampus (17.9 fmol/mg) and frontal cortex (8.6 fmol/mg) was similar as compared to specific [^{3}H]MDL 100907 binding.

Discussion

In this study we demonstrated that receptor binding of the new 5-HT$_{2A}$ receptor agonist radioligand [^{11}C]Cimbi-36 can be quantified using kinetic modeling. The cerebellum was found a suitable reference region for estimation of nondisplaceable binding, allowing the use of noninvasive reference tissue models. The mean cortical BP_{ND} estimate (SRTM) of [^{11}C]Cimbi-36 was 1.43 ± 0.27 and approximately 56% of the corresponding BP_{ND} of [^{11}C]MDL 100907. The distribution of [^{11}C]Cimbi-36 concentrations across brain regions was

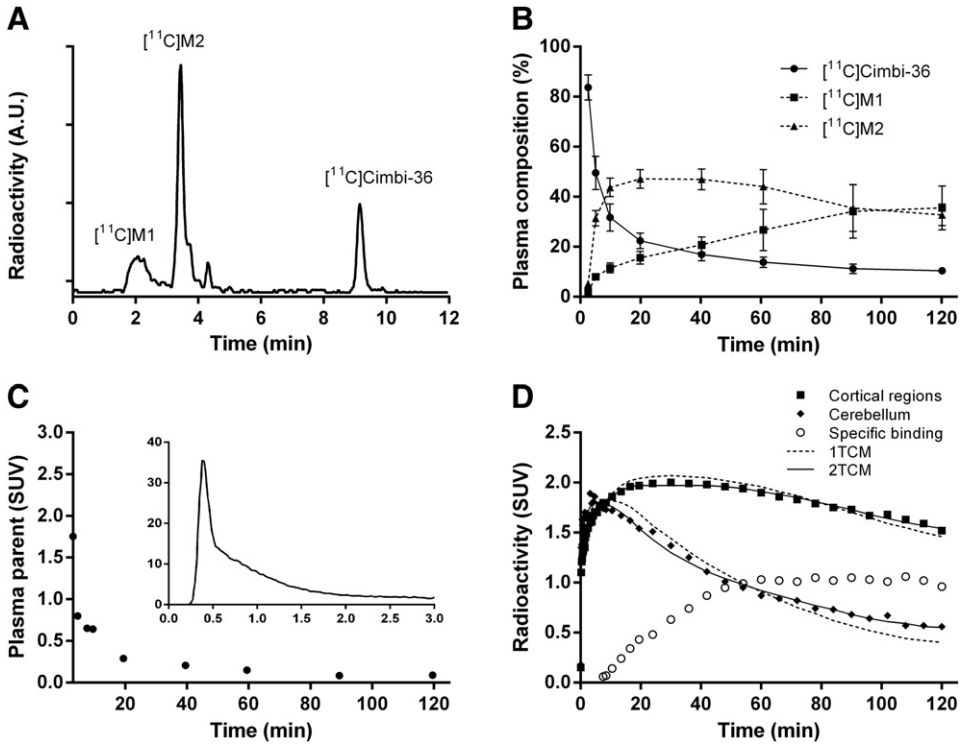

Fig. 1. Radioactivity content in plasma and brain after intravenous injection of [^{11}C]Cimbi-36 into monkey. HPLC radiochromatogram of plasma content 40 min after [^{11}C]Cimbi-36 injection (A). Plasma composition of unchanged radioligand and radiometabolite fractions over time; data represented as mean ± SD (B). Representative metabolite-corrected arterial input function of [^{11}C]Cimbi-36 (C). Representative time activity course for regional brain radioactivity and curve fitting with the 1TCM and 2TCM (D). Abbreviation, A.U. arbitrary unit.

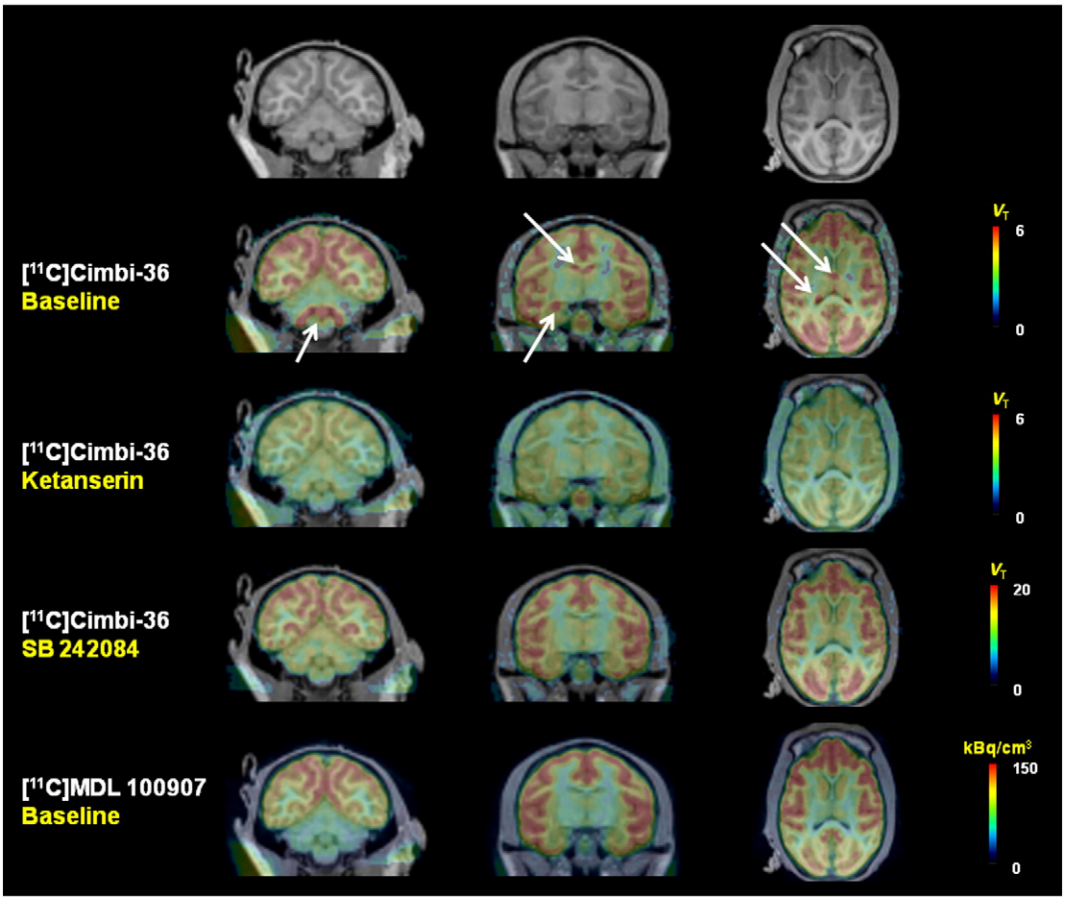

Fig. 2. MR images (top) and corresponding fused PET/MR images of [^{11}C]Cimbi-36 and [^{11}C]MDL 100907 at the level of the fourth ventricle (left), hippocampus (middle) and thalamus (right). V_T maps are presented for [^{11}C]Cimbi-36 binding during baseline conditions and after pretreatment with ketanserin or SB 242084. Summation images (average of the frames from 9 to 123 min) are presented for [^{11}C]MDL 100907 during baseline conditions. Arrows indicate high [^{11}C]Cimbi-36 binding in the choroid plexus.

different than that of [^{11}C]MDL 100907, with high [^{11}C]Cimbi-36 binding in the choroid plexus. This suggests a difference in receptor binding profile. Blocking studies with ketanserin and SB 242084 show that these differences are likely related to 5-HT$_{2C}$ receptor binding of [^{11}C]Cimbi-36. In conclusion, [^{11}C]Cimbi-36 is the first agonist radioligand available for evaluation of 5-HT$_{2A}$ receptors in the cortical regions and of 5-HT$_{2C}$ receptors in the choroid plexus of the primate brain.

After injection of [^{11}C]Cimbi-36 in rhesus monkeys, the radioactivity concentration was high in the cortical regions and lower in hippocampus and amygdala. Low concentrations of radioactivity were observed in the striatum, midbrain and cerebellum. This rank order of the radioactivity

Table 1
Comparison of the one- and two-tissue compartment model for description of [^{11}C]Cimbi-36 receptor binding in the cortical regions, choroid plexus and cerebellum of 5 PET measurements in three nonhuman primates.

			1TCM				2TCM					
Day	Subject	Brain region	K_1 (mL/cm^3/min)	k_2 (min^{-1})	SS	AIC	K_1 (mL/cm^3/min)	k_2 (min^{-1})	k_3 (min^{-1})	k_4 (min^{-1})	SS	AIC
1	NHP1	Cortical regions	0.14	0.01	158	6	0.15	0.04	0.08	0.03	30	−60
		Choroid plexus	0.17	0.02	1216	87	0.26	0.50	0.73	0.04	916	79
		Cerebellum	0.14	0.03	154	38	0.14	0.05	0.01	0.02	43	−13
2	NHP2	Cortical regions	0.09	0.01	84	−20	0.10	0.03	0.05	0.03	21	−75
		Choroid plexus	0.14	0.02	821	57	0.18	0.20	0.37	0.04	454	36
		Cerebellum	0.11	0.03	262	48	0.11	0.05	0.01	0.02	101	12
3	NHP3	Cortical regions	0.12	0.01	19	−63	0.12	0.01	0.02	0.03	9	−90
		Choroid plexus	0.20	0.01	467	43	0.20	0.02	0.02	0.04	434	45
		Cerebellum	0.14	0.03	145	40	0.15	0.05	0.04	0.05	73	16
4	NHP3	Cortical regions	0.11	0.01	96	19	0.16	0.48	0.80	0.03	21	−42
		Choroid plexus	0.17	0.02	330	42	0.18	0.02	0.01	0.01	242	34
		Cerebellum	0.12	0.03	121	51	0.13	0.06	0.03	0.03	49	17
5	NHP2	Cortical regions	0.16	0.01	83	−37	0.16	0.02	0.03	0.03	30	−75
		Choroid plexus	0.21	0.02	703	43	0.23	0.03	0.02	0.02	449	28
		Cerebellum	0.17	0.03	207	26	0.17	0.04	0.02	0.04	142	16

AIC, Akaike information criterion; NHP, nonhuman primate; SS, residual sum of squares; 1TCM, one-tissue compartment model; 2TCM, two-tissue compartment model.

Table 2
Total volumes of distribution obtained by the 1TCM and 2TCM and Logan graphical analysis (GA) with arterial input function, and binding potential values obtained with the 2TCM, GA and the simplified reference tissue model.

	Total volume of distribution, V_T (mL/cm^3)			Binding potential, BP_{ND}			
Brain region	1TCM	2TCM	GA	2TCM	GA	NIGA	SRTM
Cingulate cortex	13.3 ± 3.1	15.3 ± 4.3	13.7 ± 2.8	2.23 ± 0.56	2.06 ± 0.29	1.72 ± 0.30	1.69 ± 0.29
Insular cortex	13.3 ± 2.8	14.6 ± 2.7	12.5 ± 2.3	2.13 ± 0.44	1.81 ± 0.29	1.58 ± 0.30	1.76 ± 0.35
Temporal cortex	13.1 ± 3.2	14.7 ± 3.8	13.6 ± 3.0	2.11 ± 0.39	2.04 ± 0.32	1.60 ± 0.27	1.56 ± 0.29
Dorsolateral prefrontal cortex	12.5 ± 2.7	13.5 ± 3.0	12.9 ± 2.6	1.86 ± 0.34	1.89 ± 0.31	1.53 ± 0.30	1.50 ± 0.29
Cortical regions	12.2 ± 2.8	13.5 ± 3.3	12.7 ± 2.7	1.85 ± 0.39	1.83 ± 0.30	1.48 ± 0.28	1.43 ± 0.27
Orbital prefrontal cortex	11.9 ± 2.5	13.3 ± 2.8	12.3 ± 2.3	1.84 ± 0.37	1.75 ± 0.31	1.46 ± 0.32	1.47 ± 0.32
Parietal cortex	11.9 ± 2.9	13.1 ± 3.4	12.0 ± 2.9	1.78 ± 0.45	1.68 ± 0.36	1.37 ± 0.31	1.33 ± 0.28
Choroid plexus	11.5 ± 2.5	13.3 ± 3.7	10.8 ± 2.4	1.87 ± 0.82	1.41 ± 0.30	1.30 ± 0.23	1.40 ± 0.22
Occipital cortex	10.9 ± 2.5	11.4 ± 2.6	11.1 ± 2.4	1.41 ± 0.28	1.47 ± 0.25	1.20 ± 0.23	1.17 ± 0.23
Hippocampus	9.9 ± 2.1	10.3 ± 2.1	9.3 ± 1.6	1.19 ± 0.10	1.08 ± 0.06	0.94 ± 0.10	1.00 ± 0.10
Amygdala	7.8 ± 1.9	8.6 ± 2.1	7.3 ± 1.8	0.84 ± 0.35	0.62 ± 0.22	0.54 ± 0.21	0.72 ± 0.22
Thalamus	6.4 ± 1.8	6.7 ± 1.7	6.5 ± 1.7	0.41 ± 0.18	0.44 ± 0.17	0.38 ± 0.14	0.38 ± 0.13
Striatum	6.2 ± 1.4	7.1 ± 1.6	6.5 ± 1.3	0.50 ± 0.11	0.45 ± 0.06	0.38 ± 0.07	0.38 ± 0.08
Midbrain	5.3 ± 1.2	6.2 ± 0.9	5.5 ± 1.1	0.34 ± 0.23	0.23 ± 0.07	0.20 ± 0.10	0.24 ± 0.10
Cerebellum	4.3 ± 0.9	4.7 ± 0.8	4.5 ± 0.8				

GA, Logan graphical analysis; NIGA, noninvasive Logan graphical analysis; SRTM, simplified reference tissue model; 1TCM, one-tissue compartment model; 2TCM, two-tissue compartment model. Values are presented as mean ± S.D.; $n = 5$.

distribution is in good agreement with the previous [^{11}C]Cimbi-36 pig study (Ettrup et al., 2011) and with the known 5-HT$_{2A}$ receptor distribution reported in autoradiographic studies (Hall et al., 2000; Lopez-Gimenez et al., 1998, 2001b).

Kinetic modeling of [^{11}C]Cimbi-36 was performed using the metabolite-corrected arterial input function. The rate of [^{11}C]Cimbi-36 metabolism in nonhuman primates was rapid, with approximately 20% [^{11}C]Cimbi-36 fraction remaining after 20 min, which is similar as in pig (Ettrup et al., 2011). The observed radiometabolites eluted earlier from the reversed-phase column than [^{11}C]Cimbi-36, suggesting that the radiometabolites are more polar and therefore less likely to pass the blood–brain-barrier. The f_p of [^{11}C]Cimbi-36 was lower than for [^{11}C]MDL 100907 (0.05 vs. 0.5, respectively) but still of sufficient size to allow reliable quantification of the free [^{11}C]Cimbi-36 concentration in plasma.

The cerebellum has in autoradiographic studies been shown to contain negligible amounts of 5-HT$_{2A}$ receptors (Hall et al., 2000; Lopez-Gimenez et al., 2001b). Application of the cerebellum as a reference region for estimation of nondisplaceable binding has been successful for studies using other 5-HT$_{2A}$ receptor radioligands, such as [^{18}F]altanserin (Pinborg et al., 2003) and [^{11}C]MDL 100907 (Talbot et al., 2012). In the current study the time course of radioactivity in the cerebellum was best described with the 2TCM. Importantly, we here demonstrated that administration of high doses of the 5-HT$_2$ receptor antagonist

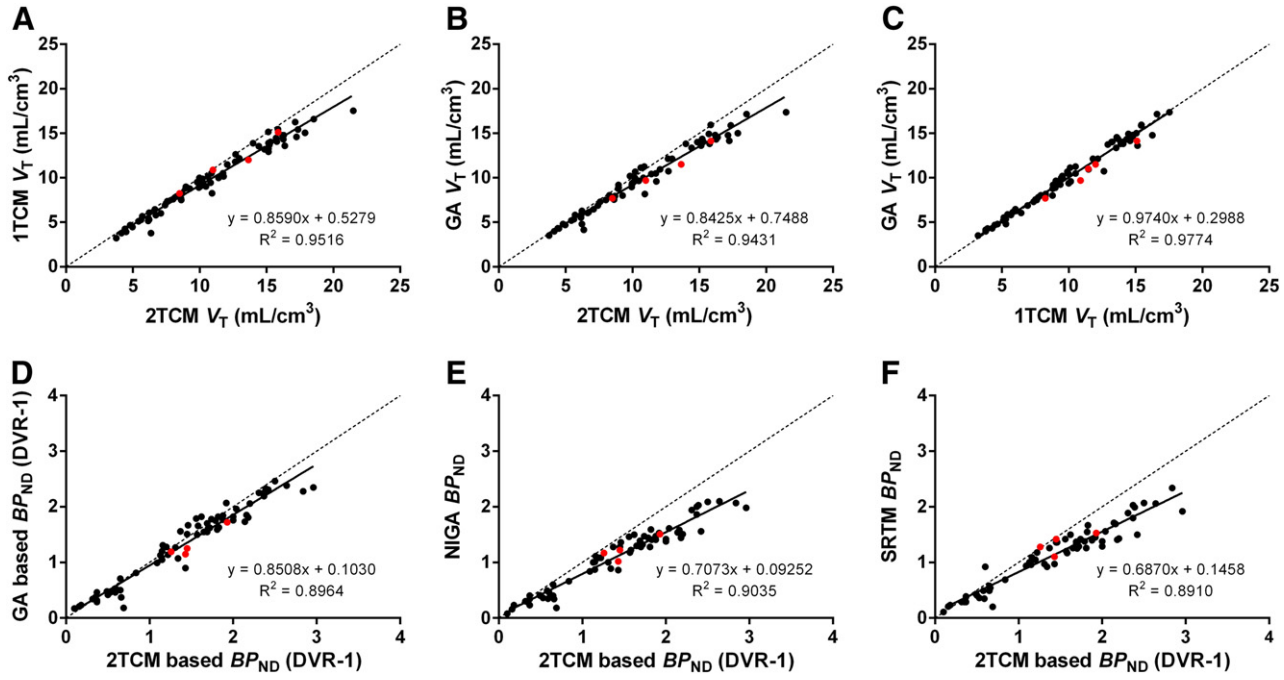

Fig. 3. Correlations of the outcome measures V_T and BP_{ND} derived by different nonlinear and linear models. Correlation between V_T estimates obtained by the 2TCM and the 1TCM (A). Correlation between V_T estimates obtained by the 2TCM and the GA (B). Correlation between V_T estimates obtained by the 1TCM and the GA (C). Correlation between BP_{ND} estimates obtained by the 2TCM and the GA (D). Correlation between BP_{ND} estimates obtained by the 2TCM and the NIGA (E). Correlation between BP_{ND} estimates obtained by the 2TCM and the SRTM (F). The solid lines represent linear regression analysis and dotted lines represent the line of identity. Results of regression analysis included 15 regions of five baseline PET measurements in three nonhuman primates. Red symbols represent the choroid plexus.

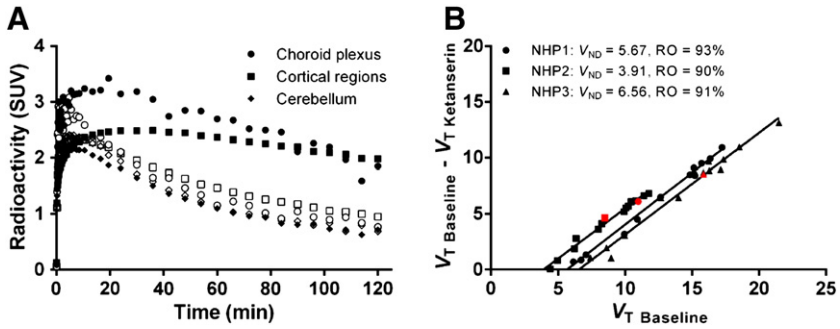

Fig. 4. Mean time activity course for regional brain radioactivity (SUV) in choroid plexus, cortical regions and cerebellum during baseline (closed symbols) and after pretreatment with ketanserin (open symbols) before injection of [^{11}C]Cimbi-36 in three rhesus monkeys (A). Lassen plots using V_T values obtained during baseline conditions and after ketanserin pretreatment before injection of [^{11}C]Cimbi-36 in three nonhuman primates (B). Regression analysis included 14 regions; with red symbols representing the choroid plexus. V_{ND} values represent the intercepts with the x-axis and receptor occupancy (RO) values were derived from the slope of the linear regression analyses.

ketanserin did not affect cerebellar V_T values. Moreover, the V_{ND} values obtained with the corresponding Lassen plots, were not significantly different than the cerebellar V_T estimates (paired *t*-test). The cerebellum contains thus no [^{11}C]Cimbi-36 binding specific to 5-HT$_2$ receptors and is a suitable reference region for estimation of nondisplaceable [^{11}C]Cimbi-36 binding in the nonhuman primate brain.

In all examined brain regions, the peak in specific binding, defined as the difference between radioactivity in the target region and the cerebellum, was achieved during the PET examination. It can thus be concluded that the transient equilibrium was achieved during the PET examinations and that the time course of regional radioactivity may be best described by kinetic models assuming reversible binding. Compartmental analysis of regional brain radioactivity concentrations using the [^{11}C]Cimbi-36 input function demonstrated that the 2TCM provided statistically better fits than the 1TCM for all brain regions. Although the individual rate parameters (k_2, k_3 and k_4) and the k_3/k_4 ratio were highly variable and could not be reliably estimated, the 2TCM provided reliable estimates of V_T. V_T values obtained with the GA corresponded with the 2TCM estimates and confirmed reversible binding by demonstrating a linear phase for all brain regions.

Reference region approaches have the advantage of not requiring an arterial input function and thereby facilitate the application of radioligands into the clinical setting. We here explored two reference region models, the NIGA and the SRTM. BP_{ND} values of both models correlated well with BP_{ND} values obtained with kinetic modeling, although a negative bias was observed in brain regions with relative high BP_{ND} values. This discrepancy in BP_{ND} values has previously also been observed for other radioligands with a reference region which best fitted with the 2TCM. This bias has been proposed to be related to violation of the SRTM assumption that the time course of radioactivity in the reference region can be described by the 1TCM (Slifstein et al., 2000). Considering the advantages of reference region approaches, typically including higher test–retest reproducibility and lower inter subject variability, and the redundancy of an arterial input function, we propose that the SRTM can be considered suitable for use in future studies.

The specificity of [^{11}C]Cimbi-36 binding to 5-HT$_2$ receptors was demonstrated by administrating the 5-HT$_2$ receptor antagonist ketanserin before injection of [^{11}C]Cimbi-36. The initial applied ketanserin dose of 1.5 mg/kg resulted in significant cardiovascular effects and we therefore lowered the dose to 0.75 mg/kg in the remaining two animals. The receptor occupancy of both ketanserin doses yielded high receptor occupancy (>80%). Corresponding Lassen plots demonstrated suitable linear regression analyses ($R^2 > 0.98$), indicating homogenous receptor occupancy across brain regions. Thus [^{11}C]Cimbi-36 binds in a reversible manner to 5-HT$_2$ receptors in the nonhuman primate brain.

To evaluate potential differences in receptor binding of an agonist and antagonist 5-HT$_{2A}$ receptor radioligand, we compared [^{11}C]Cimbi-36 and [^{11}C]MDL 100907. The binding potentials of [^{11}C]Cimbi-36 were lower than for [^{11}C]MDL 100907, with cortical BP_{ND} values being 56% of [^{11}C]MDL 100907. Although this rank order is consistent with the 5-HT$_2$ receptor affinities (K_D) of 0.2–0.6 nM for [^{11}C]MDL 100907 (Johnson et al., 1996; Lopez-Gimenez et al., 1998) and of 1.3 nM for [^{11}C]Cimbi-36 (see Supplementary Fig. 2), these differences in BP_{ND} estimates may also be related to nonspecific binding, density of available receptors or to competition with endogenous serotonin.

A major difference between [^{11}C]Cimbi-36 and [^{11}C]MDL 100907 binding was high [^{11}C]Cimbi-36 binding in the choroid plexus. The

Table 3
Total volumes of distribution obtained by the 2TCM and binding potential values obtained with the 2TCM and the simplified reference tissue model after injection of [^{11}C]Cimbi-36 during baseline conditions and after pretreatment with ketanserin.

	2TCM									SRTM		
	Total volume of distribution, V_T			Binding potential, BP_F			Binding potential, BP_{ND}			Binding potential, BP_{ND}		
Brain region	Bsln	KET	Change (%)	Bsln	KET	Change (%)	Bsln	KET	Change (%)	Bsln	KET	Change (%)
Cortical regions	14.1 ± 3.7	6.1 ± 1.5	−56 ± 1	238 ± 148	28 ± 15	−88 ± 1	2.07 ± 0.33	0.32 ± 0.07	−85 ± 1	1.61 ± 0.29	0.27 ± 0.05	−83 ± 3
Choroid plexus	11.8 ± 3.8	5.3 ± 1.8	−55 ± 1	186 ± 143	15 ± 21	−94 ± 5	1.55 ± 0.34	0.14 ± 0.16	−92 ± 8	1.30 ± 0.19	0.09 ± 0.06	−93 ± 3
Hippocampus	10.2 ± 2.4	5.8 ± 1.3	−43 ± 10	141 ± 90	20 ± 11	−83 ± 11	1.23 ± 0.10	0.26 ± 0.17	−79 ± 14	0.99 ± 0.09	0.23 ± 0.08	−77 ± 6
Amygdala	9.0 ± 2.5	5.9 ± 1.4	−34 ± 6	108 ± 58	23 ± 10	−78 ± 3	0.98 ± 0.40	0.27 ± 0.09	−72 ± 2	0.62 ± 0.26	0.19 ± 0.05	−66 ± 11
Striatum	6.9 ± 1.8	5.5 ± 1.3	−19 ± 3	60 ± 44	16 ± 8	−69 ± 8	0.50 ± 0.15	0.19 ± 0.05	−61 ± 4	0.38 ± 0.10	0.14 ± 0.03	−61 ± 9
Thalamus	6.7 ± 2.3	6.0 ± 1.8	−9 ± 6	58 ± 55	27 ± 22	−39 ± 33	0.44 ± 0.24	0.29 ± 0.12	−25 ± 30	0.41 ± 0.18	0.24 ± 0.12	−40 ± 17
Midbrain	6.6 ± 0.7	5.1 ± 1.4	−23 ± 18	48 ± 17	9 ± 10	−80 ± 21	0.48 ± 0.19	0.09 ± 0.11	−73 ± 27	0.25 ± 0.08	0.10 ± 0.10	−64 ± 32
Cerebellum	4.6 ± 0.8	4.6 ± 0.9	1 ± 3									

Bsln, baseline; KET, ketanserin; SRTM, simplified reference tissue model; 2TCM, two-tissue compartment model. Values are presented as mean ± S.D.; $n = 3$.

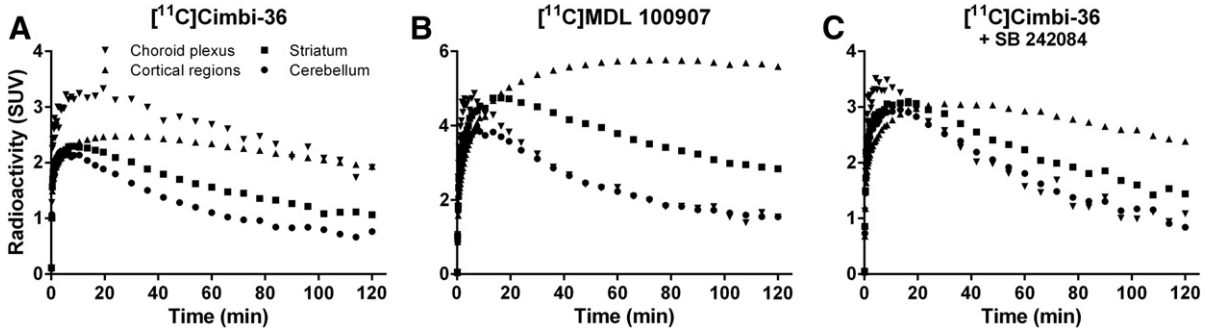

Fig. 5. Mean time activity course for regional brain radioactivity (SUV) in choroid plexus, cortical regions, striatum and cerebellum after injection of [^{11}C]Cimbi-36 ($n = 5$) (A) or [^{11}C]MDL 100907 ($n = 4$) (B) in rhesus monkeys. Mean time activity course for regional brain radioactivity in choroid plexus, cortical regions, striatum and cerebellum after pretreatment with SB 242084 before injection of [^{11}C]Cimbi-36 in two rhesus monkeys (C).

choroid plexus is the blood-cerebrospinal fluid barrier and is present in several parts of the ventricular system. High [^{11}C]Cimbi-36 binding was observed in the lateral, third and fourth ventricles (Figs. 2 and 7). Autoradiographic studies using [^{3}H]mesulergine have previously demonstrated that the choroid plexus contains a high density (625 ± 106 fmol/mg protein) of 5-HT$_{2C}$ receptors in the primate brain (Lopez-Gimenez et al., 2001a; Marazziti et al., 1999). In vitro, [^{11}C]Cimbi-36 has been shown to be only marginally selective towards 5-HT$_{2A}$ over 5-HT$_{2C}$ receptors (K_i (nM): 5-HT$_{2A}$ = 0.5-0.8; 5-HT$_{2B}$ = 0.5; 5-HT$_{2C}$ = 1.7 (Ettrup et al., 2011). Furthermore, [^{11}C]MDL 100907 provided no specific binding in the choroid plexus, further supporting that this region is devoid of 5-HT$_{2A}$ receptors, and we therefore evaluated the suitability of [^{11}C]Cimbi-36 to quantify selectively 5-HT$_{2C}$ receptor binding in the choroid plexus.

The binding of [^{11}C]Cimbi-36 in the choroid plexus was examined by defining a VOI on the fourth ventricle using fused PET/MR images. We found that the time course of radioactivity in the choroid plexus was best described by the 2TCM. The obtained vB and K_1 values were higher than in other brain regions, which is consistent with the choroid plexus tissue being highly vascularized. More accurate definition of the choroid plexus, using e.g. dedicated MRI techniques, may improve the accuracy of the quantification of [^{11}C]Cimbi-36 binding parameters in future studies.

Administration of the 5-HT$_2$ receptor antagonist ketanserin (~8× selectivity of 5-HT$_{2A}$ towards 5-HT$_{2C}$ (K_i (nM)) (Knight et al., 2004)) or the 5-HT$_{2C}$ receptor antagonist SB 242084 (~120× selectivity of 5-HT$_{2C}$ towards 5-HT$_{2A}$ (K_i (nM)) (Knight et al., 2004)) reduced the binding in choroid plexus to the level of the cerebellum. These results confirm that [^{11}C]Cimbi-36 binds specifically 5-HT$_{2C}$ receptors in the choroid plexus and suggest the potential of cerebellum as reference region. Indeed, V_T and BP_{ND} estimates obtained for the choroid plexus after [^{11}C]Cimbi-36 injection correlated across quantification models in a similar manner as for other brain regions (Fig. 3). The binding of [^{11}C]Cimbi-36 in the choroid plexus may thus potentially be quantified using cerebellum as reference region, and further validation of this appealing modeling approach is warranted.

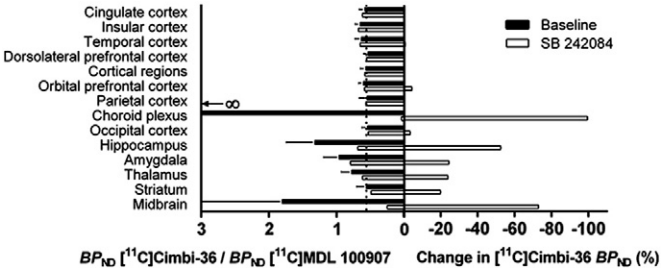

Fig. 6. (Left) Relative [^{11}C]Cimbi-36 binding obtained during baseline conditions ($n = 4$; mean ± SD) and after pretreatment with SB 242084 ($n = 2$; mean) in rhesus monkeys. The binding of [^{11}C]Cimbi-36 was expressed relative to [^{11}C]MDL 100907 binding obtained during baseline conditions (BP_{ND} [^{11}C]Cimbi-36 [baseline or SB 242084]/BP_{ND} [^{11}C]MDL 100907 [baseline]). BP_{ND} values were estimated with the SRTM. The dotted line represents the mean ratio obtained in the cortical regions during baseline conditions. (Right) Mean relative change in BP_{ND} after pretreatment with SB 242084 before injection of [^{11}C]Cimbi-36 in two rhesus monkeys.

The ratio of [^{11}C]Cimbi-36 over [^{11}C]MDL 100907 binding was heterogeneous across brain regions. The majority of cortical regions have previously been shown devoid of 5-HT$_{2C}$ receptors in vitro (Marazziti et al., 1999) and administration of SB 242084 did indeed not affect [^{11}C]Cimbi-36 binding in cortical regions. The ratio of [^{11}C]Cimbi-36 over [^{11}C]MDL 100907 binding in the midbrain, hippocampus, amygdala and thalamus was found higher than in the cortical regions. A potential interpretation for this higher [^{11}C]Cimbi-36 binding is that these regions contain a higher fraction of receptors in the high-affinity receptor state. However, administration of SB 242084 reduced [^{11}C]Cimbi-36 binding, in particular, in these brain regions, suggesting that the regional differences in relative [^{11}C]Cimbi-36 binding are likely 5-HT$_{2C}$ receptor-related.

Membrane homogenate and autoradiographic studies have previously demonstrated that 5-HT$_{2C}$ receptors are present in the substantia nigra, basal ganglia, amygdala, hippocampus and hypothalamus of the primate brain (Lopez-Gimenez et al., 2001a; Marazziti et al., 1999). The abundance of the 5-HT$_{2C}$ receptors in these brain regions is however considerably lower than in the choroid plexus, ~15 vs. 625 fmol/mg protein, respectively (Marazziti et al., 1997, 1999). Literature on a direct comparison of the 5-HT$_{2A}$ and 5-HT$_{2C}$ receptor densities is scarce, due to the lack of selective 5-HT$_{2C}$ radioligands, but Marazziti et al. have reported that the 5-HT$_{2C}$ receptor density is about 10-fold lower than the 5-HT$_{2A}$ receptor density in the striatum and hippocampus (Marazziti et al., 1997, 1999). The observed SB 242084-induced decrease in hippocampal [^{11}C]Cimbi-36 BP_{ND} was 40–65%, and is not consistent with a 5-HT$_{2C}$ receptor fraction of 10% in this region. An important contribution to this inconsistency may come from spill-in effects from choroid plexus tissue located in nearby ventricles. In fact, the majority of regions displaying 5-HT$_{2C}$ receptor specific binding are located in the proximity of the ventricular system (Fig. 2). It can therefore not be ruled out that [^{11}C]Cimbi-36 binding in the brain only reflects 5-HT$_{2C}$ receptors in the choroid plexus, while other brain regions represent 5-HT$_{2A}$ receptor binding. Future studies in human subjects may provide further understanding of the regional 5-HT$_{2C}$ receptor contribution to [^{11}C]Cimbi-36 binding and benefit from the larger brain volumes and reduced spill-in confounding effects.

The 5-HT$_{2C}$ receptor is thought implicated in aging and several neuropsychiatric disorders, including obesity, depression, schizophrenia and drug abuse. Recently approved drugs targeting the 5-HT$_{2C}$ receptor include the agonist lorcaserin (Smith et al., 2008; Thomsen et al., 2008),

Table 4
Total volumes of distribution obtained by the 2TCM and binding potential values obtained with the 2TCM and the simplified reference tissue model after injection of [^{11}C]Cimbi-36 during baseline conditions and after pretreatment with SB 242084.

	2TCM									SRTM		
	Total volume of distribution, V_T			Binding potential, BP_F			Binding potential, BP_{ND}			Binding potential, BP_{ND}		
Brain region	Bsln	SB 242084	Change (%)	Bsln	SB 242084	Change (%)	Bsln	SB 242084	Change (%)	Bsln	SB 242084	Change (%)
Cortical regions	12.5	25.0	101	139	139	5	1.53	1.19	−21	1.25	1.27	2
Choroid plexus	15.7	11.4	−24	200	1	−99	2.35	0.01	−100	1.38	0.00	−100
Hippocampus	10.4	15.2	46	101	39	−60	1.12	0.34	−70	0.95	0.70	−26
Amygdala	8.0	15.6	96	56	43	−20	0.62	0.37	−40	0.71	0.48	−25
Striatum	7.4	15.7	114	46	46	7	0.51	0.39	−22	0.40	0.29	−26
Thalamus	6.6	14.4	113	32	29	−11	0.36	0.25	−30	0.34	0.25	−24
Midbrain	5.5	11.4	108	11	6	−55	0.13	0.05	−70	0.16	0.06	−73
Cerebellum	4.9	11.4	132									

Bsln, baseline; SRTM, simplified reference tissue model; 2TCM, two-tissue compartment model. Values are presented as mean; $n = 2$.

in 2012 FDA-approved as a weight-loss drug, and the antagonist agomelatine (Loo et al., 2002; Millan et al., 2003), which is approved for depression. As the earlier attempts for development of a 5-HT$_{2C}$ receptor selective PET radioligand have been unsuccessful (Granda et al., 2013), [^{11}C]Cimbi-36 may thus provide the first opportunity for evaluation of the role of 5-HT$_{2C}$ receptors in several neuropsychiatric disorders and their treatments.

[^{11}C]Cimbi-36 was initially developed as an agonist radioligand for 5-HT$_{2A}$ receptors. An anticipated advantage of the agonistic properties is an enhanced sensitivity to endogenous serotonin concentrations. Indeed, preliminary experiments in monkey suggest that [^{11}C]Cimbi-36 binding is sensitive to fenfluramine-induced changes in serotonin concentrations (Finnema et al., 2011). Future studies need to confirm that [^{11}C]Cimbi-36 has additional value to other radioligands, such as [^{11}C]CUMI-101 and [^{11}C]AZ10419369, which have recently been found suitable for PET imaging of serotonin release in the living brain (Finnema et al., 2010; Milak et al., 2011; Nord et al., 2013; Selvaraj et al., 2012).

In conclusion, [^{11}C]Cimbi-36 provides reversible binding to 5-HT$_{2A}$ and 5-HT$_{2C}$ receptors in the nonhuman primate brain which can be quantified using PET. Application of [^{11}C]Cimbi-36 in human subjects is warranted and it is anticipated that [^{11}C]Cimbi-36 has unique properties which make it a valuable tool for studies on the pathophysiology and treatment of patients suffering from neuropsychiatric disorders.

Acknowledgments

The authors thank the members of the PET group at the Karolinska Institutet for excellent assistance; in particular Gudrun Nylén and Siv Eriksson for assistance with the PET and autoradiography studies, respectively. We also thank Dr. Andrea Varrone for scientific discussions during the start of this study. The Lundbeck Foundation supported Anders Ettrup through a centre grant (Cimbi).

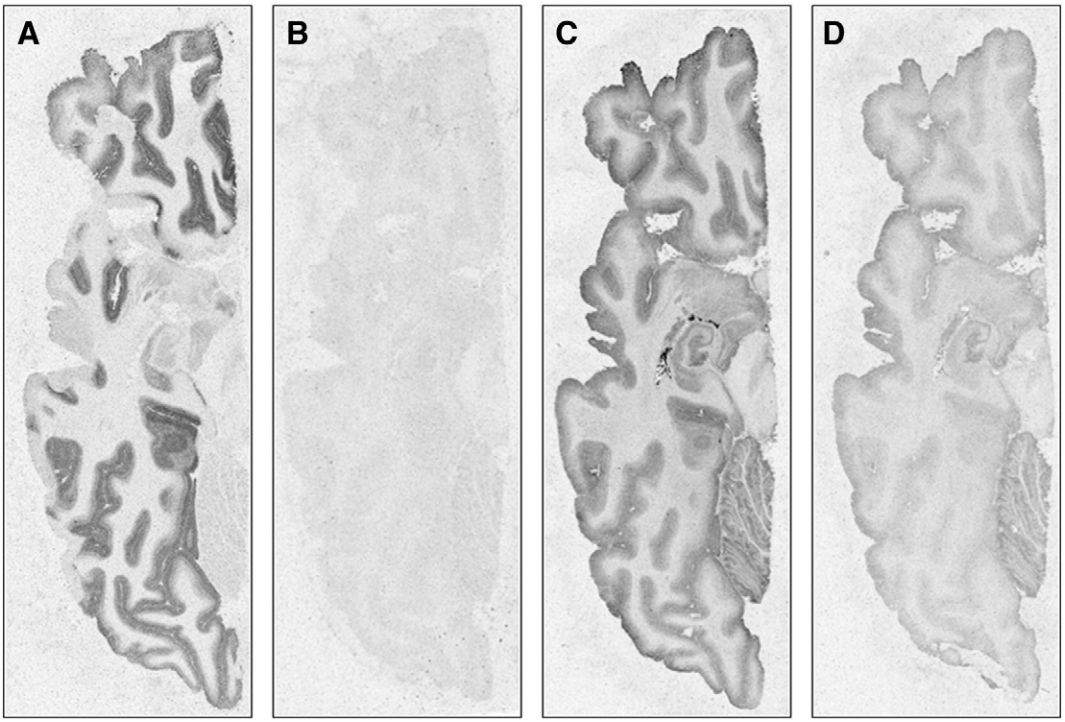

Fig. 7. Autoradiograms showing [^{3}H]MDL 100907 (A–B) and [^{3}H]Cimbi-36 (C–D) binding in transaxial human whole hemisphere sections. Autoradiographic images depicting total (A) [^{3}H]MDL 100907 binding and total (C) [^{3}H]Cimbi-36 binding at 0.5 nM. Nonspecific binding (B and D) was applied in the presence of 10 μM ketanserin.

Appendix A. Supplementary data

Supplementary data to this article can be found online at http://dx.doi.org/10.1016/j.neuroimage.2013.08.035.

References

Adams, K.H., Hansen, E.S., Pinborg, L.H., Hasselbalch, S.G., Svarer, C., Holm, S., Bolwig, T.G., Knudsen, G.M., 2005. Patients with obsessive–compulsive disorder have increased 5-HT2A receptor binding in the caudate nuclei. Int. J. Neuropsychopharmacol. 8 (3), 391–401.

Akaike, H., 1974. A new look at the statistical model identification. IEEE Trans. Autom. Control 19, 716–723.

Andersson, J., Truong, P., Halldin, C., 2009. In-target produced [11C]methane: increased specific radioactivity. Appl. Radiat. Isot. 67 (1), 106–110.

Andersson, J.D., Varnas, K., Cselenyi, Z., Gulyas, B., Wensbo, D., Finnema, S.J., Swahn, B.M., Svensson, S., Nyberg, S., Farde, L., Halldin, C., 2010. Radiosynthesis of the candidate beta-amyloid radioligand [(11)C]AZD2184: positron emission tomography examination and metabolite analysis in cynomolgus monkeys. Synapse 64 (10), 733–741.

Biver, F., Goldman, S., Luxen, A., Monclus, M., Forestini, M., Mendlewicz, J., Lotstra, F., 1994. Multicompartmental study of fluorine-18 altanserin binding to brain 5HT2 receptors in humans using positron emission tomography. Eur. J. Nucl. Med. 21 (9), 937–946.

Bromidge, S.M., Duckworth, M., Forbes, I.T., Ham, P., King, F.D., Thewlis, K.M., Blaney, F.E., Naylor, C.B., Blackburn, T.P., Kennett, G.A., Wood, M.D., Clarke, S.E., 1997. 6-Chloro-5-methyl-1-[[2-[(2-methyl-3-pyridyl)oxy]-5-pyridyl]carbamoyl]-indoline (SB-242084): the first selective and brain penetrant 5-HT2C receptor antagonist. J. Med. Chem. 40 (22), 3494–3496.

Carson, R.E., 1986. Parameter estimation in PET. In: Phelps, M.J.M., Schelbert, H. (Eds.), Positron Emission Tomography and Autoradiography: Principles and Applications for the Brain and the Heart. Raven Press, New York, USA, pp. 287–346.

Erritzoe, D., Frokjaer, V.G., Haugbol, S., Marner, L., Svarer, C., Holst, K., Baare, W.F., Rasmussen, P.M., Madsen, J., Paulson, O.B., Knudsen, G.M., 2009. Brain serotonin 2A receptor binding: relations to body mass index, tobacco and alcohol use. NeuroImage 46 (1), 23–30.

Ettrup, A., Palner, M., Gillings, N., Santini, M.A., Hansen, M., Kornum, B.R., Rasmussen, L.K., Nagren, K., Madsen, J., Begtrup, M., Knudsen, G.M., 2010. Radiosynthesis and evaluation of 11C-CIMBI-5 as a 5-HT2A receptor agonist radioligand for PET. J. Nucl. Med. 51 (11), 1763–1770.

Ettrup, A., Hansen, M., Santini, M.A., Paine, J., Gillings, N., Palner, M., Lehel, S., Herth, M.M., Madsen, J., Kristensen, J., Begtrup, M., Knudsen, G.M., 2011. Radiosynthesis and in vivo evaluation of a series of substituted 11C-phenethylamines as 5-HT (2A) agonist PET tracers. Eur. J. Nucl. Med. Mol. Imaging 38 (4), 681–693.

Ettrup, A., Holm, S., Hansen, M., Wasim, M., Santini, M.A., Palner, M., Madsen, J., Svarer, C., Kristensen, J.L., Knudsen, G.M., 2013. Preclinical safety assessment of the 5-HT2A receptor agonist PET radioligand [(11)C]Cimbi-36. Mol. Imaging Biol. 15 (4), 376–383.

Finnema, S.J., Varrone, A., Hwang, T.J., Gulyas, B., Pierson, M.E., Halldin, C., Farde, L., 2010. Fenfluramine-induced serotonin release decreases [11C]AZ10419369 binding to 5-HT1B-receptors in the primate brain. Synapse 64 (7), 573–577.

Finnema, S.J., Ettrup, A., Stepanov, V., Nakao, R., Yamamoto, S., Varrone, A., Knudsen, G., Halldin, C., 2011. Pilot study on receptor binding and serotonin sensitivity of [11C] CIMBI-36 in monkey brain. J. Nucl. Med. 52 (S1), 495.

Fitzgerald, L.W., Conklin, D.S., Krause, C.M., Marshall, A.P., Patterson, J.P., Tran, D.P., Iyer, G., Kostich, W.A., Largent, B.L., Hartig, P.R., 1999. High-affinity agonist binding correlates with efficacy (intrinsic activity) at the human serotonin 5-HT2A and 5-HT2C receptors: evidence favoring the ternary complex and two-state models of agonist action. J. Neurochem. 72 (5), 2127–2134.

Garber, J.C., Barbee, R.W., Bielitzki, J.T., Clayton, L.A., Donovan, J.C., Hendriksen, C.F.M., Kohn, D.F., Lipman, N.S., Locker, P.A., Melcher, J., Quimby, F.W., Turner, P.V., Wood, G.A., Wurbel, H., 2011. Guide for the Care and Use of Laboratory Animals. The National Academies Press, Washington D.C., USA.

Ginovart, N., Galineau, L., Willeit, M., Mizrahi, R., Bloomfield, P.M., Seeman, P., Houle, S., Kapur, S., Wilson, A.A., 2006. Binding characteristics and sensitivity to endogenous dopamine of [11C]-(+)-PHNO, a new agonist radiotracer for imaging the high-affinity state of D2 receptors in vivo using positron emission tomography. J. Neurochem. 97 (4), 1089–1103.

Granda, M.L., Carlin, S.M., Moseley, C.K., Neelamegam, R., Mandeville, J.B., Hooker, J.M., 2013. Synthesis and evaluation of methylated arylazepine compounds for PET imaging of 5-HT(2c) receptors. ACS Chem. Neurosci. 4 (2), 261–265.

Hall, H., Farde, L., Halldin, C., Lundkvist, C., Sedvall, G., 2000. Autoradiographic localization of 5-HT(2A) receptors in the human brain using [(3)H]M100907 and [(11)C] M100907. Synapse 38 (4), 421–431.

Hansen, H.D., Ettrup, A., Herth, M.M., Dyssegaard, A., Ratner, C., Gillings, N., Knudsen, G.M., 2013. Direct comparison of [(18) F]MH.MZ and [(18) F]altanserin for 5-HT2A receptor imaging with PET. Synapse 67 (6), 328–337.

Haugbol, S., Pinborg, L.H., Regeur, L., Hansen, E.S., Bolwig, T.G., Nielsen, F.A., Svarer, C., Skovgaard, L.T., Knudsen, G.M., 2007. Cerebral 5-HT2A receptor binding is increased in patients with Tourette's syndrome. Int. J. Neuropsychopharmacol. 10 (2), 245–252.

Hirani, E., Sharp, T., Sprakes, M., Grasby, P., Hume, S., 2003. Fenfluramine evokes 5-HT2A receptor-mediated responses but does not displace [11C]MDL 100907: small animal PET and gene expression studies. Synapse 50 (3), 251–260.

Hoyer, D., Martin, G., 1997. 5-HT receptor classification and nomenclature: towards a harmonization with the human genome. Neuropharmacology 36 (4–5), 419–428.

Innis, R.B., Cunningham, V.J., Delforge, J., Fujita, M., Gjedde, A., Gunn, R.N., Holden, J., Houle, S., Huang, S.C., Ichise, M., Iida, H., Ito, H., Kimura, Y., Koeppe, R.A., Knudsen, G.M., Knuuti, J., Lammertsma, A.A., Laruelle, M., Logan, J., Maguire, R.P., Mintun, M.A., Morris, E.D., Parsey, R., Price, J.C., Slifstein, M., Sossi, V., Suhara, T., Votaw, J.R., Wong, D.F., Carson, R.E., 2007. Consensus nomenclature for in vivo imaging of reversibly binding radioligands. J. Cereb. Blood Flow Metab. 27 (9), 1533–1539.

Ito, H., Nyberg, S., Halldin, C., Lundkvist, C., Farde, L., 1998. PET imaging of central 5-HT2A receptors with carbon-11-MDL 100,907. J. Nucl. Med. 39 (1), 208–214.

Johnson, M.P., Siegel, B.W., Carr, A.A., 1996. [3H]MDL 100,907: a novel selective 5-HT2A receptor ligand. Naunyn Schmiedebergs Arch. Pharmacol. 354 (2), 205–209.

Karlsson, P., Farde, L., Halldin, C., Swahn, C.G., Sedvall, G., Foged, C., Hansen, K.T., Skrumsager, B., 1993. PET examination of [11C]NNC 687 and [11C]NNC 756 as new radioligands for the D1-dopamine receptor. Psychopharmacology (Berl.) 113 (2), 149–156.

Kennett, G.A., Wood, M.D., Bright, F., Trail, B., Riley, G., Holland, V., Avenell, K.Y., Stean, T., Upton, N., Bromidge, S., Forbes, I.T., Brown, A.M., Middlemiss, D.N., Blackburn, T.P., 1997. SB 242084, a selective and brain penetrant 5-HT2C receptor antagonist. Neuropharmacology 36 (4–5), 609–620.

Kent, R.S., De Lean, A., Lefkowitz, R.J., 1980. A quantitative analysis of beta-adrenergic receptor interactions: resolution of high and low affinity states of the receptor by computer modeling of ligand binding data. Mol. Pharmacol. 17 (1), 14–23.

Knight, A.R., Misra, A., Quirk, K., Benwell, K., Revell, D., Kennett, G., Bickerdike, M., 2004. Pharmacological characterisation of the agonist radioligand binding site of 5-HT(2A), 5-HT(2B) and 5-HT(2C) receptors. Naunyn Schmiedebergs Arch. Pharmacol. 370 (2), 114–123.

Lammertsma, A.A., Hume, S.P., 1996. Simplified reference tissue model for PET receptor studies. NeuroImage 4 (3 Pt 1), 153–158.

Lemaire, C., Cantineau, R., Guillaume, M., Plenevaux, A., Christiaens, L., 1991. Fluorine-18-altanserin: a radioligand for the study of serotonin receptors with PET: radiolabeling and in vivo biologic behavior in rats. J. Nucl. Med. 32 (12), 2266–2272.

Leysen, J.E., Awouters, F., Kennis, L., Laduron, P.M., Vandenberk, J., Janssen, P.A., 1981. Receptor binding profile of R 41 468, a novel antagonist at 5-HT2 receptors. Life Sci. 28 (9), 1015–1022.

Logan, J., Fowler, J.S., Volkow, N.D., Wolf, A.P., Dewey, S.L., Schlyer, D.J., MacGregor, R.R., Hitzemann, R., Bendriem, B., Gatley, S.J., et al., 1990. Graphical analysis of reversible radioligand binding from time-activity measurements applied to [N-11C-methyl]-(−)-cocaine PET studies in human subjects. J. Cereb. Blood Flow Metab. 10 (5), 740–747.

Logan, J., Fowler, J.S., Volkow, N.D., Wang, G.J., Ding, Y.S., Alexoff, D.L., 1996. Distribution volume ratios without blood sampling from graphical analysis of PET data. J. Cereb. Blood Flow Metab. 16 (5), 834–840.

Loo, H., Hale, A., D'Haenen, H., 2002. Determination of the dose of agomelatine, a melatoninergic agonist and selective 5-HT(2C) antagonist, in the treatment of major depressive disorder: a placebo-controlled dose range study. Int. Clin. Psychopharmacol. 17 (5), 239–247.

Lopez-Gimenez, J.F., Vilaro, M.T., Palacios, J.M., Mengod, G., 1998. [3H]MDL 100,907 labels 5-HT2A serotonin receptors selectively in primate brain. Neuropharmacology 37 (9), 1147–1158.

Lopez-Gimenez, J.F., Mengod, G., Palacios, J.M., Vilaro, M.T., 2001a. Regional distribution and cellular localization of 5-HT2C receptor mRNA in monkey brain: comparison with [3H]mesulergine binding sites and choline acetyltransferase mRNA. Synapse 42 (1), 12–26.

Lopez-Gimenez, J.F., Vilaro, M.T., Palacios, J.M., Mengod, G., 2001b. Mapping of 5-HT2A receptors and their mRNA in monkey brain: [3H]MDL100,907 autoradiography and in situ hybridization studies. J. Comp. Neurol. 429 (4), 571–589.

Lopez-Gimenez, J.F., Villazon, M., Brea, J., Loza, M.I., Palacios, J.M., Mengod, G., Vilaro, M.T., 2001c. Multiple conformations of native and recombinant human 5-hydroxytryptamine(2a) receptors are labeled by agonists and discriminated by antagonists. Mol. Pharmacol. 60 (4), 690–699.

Lundkvist, C., Halldin, C., Ginovart, N., Nyberg, S., Swahn, C.G., Carr, A.A., Brunner, F., Farde, L., 1996. [11C]MDL 100907, a radioligland for selective imaging of 5-HT(2A) receptors with positron emission tomography. Life Sci. 58 (10), PL 187–PL 192.

Manvich, D.F., Kimmel, H.L., Cooper, D.A., Howell, L.L., 2012a. The serotonin 2C receptor antagonist SB 242084 exhibits abuse-related effects typical of stimulants in squirrel monkeys. J. Pharmacol. Exp. Ther. 342 (3), 761–769.

Manvich, D.F., Kimmel, H.L., Howell, L.L., 2012b. Effects of serotonin 2C receptor agonists on the behavioral and neurochemical effects of cocaine in squirrel monkeys. J. Pharmacol. Exp. Ther. 341 (2), 424–434.

Marazziti, D., Rossi, A., Palego, L., Giannaccini, G., Naccarato, A., Lucacchini, A., Cassano, G.B., 1997. [3H]ketanserin binding in human brain postmortem. Neurochem. Res. 22 (6), 753–757.

Marazziti, D., Rossi, A., Giannaccini, G., Zavaglia, K.M., Dell'Osso, L., Lucacchini, A., Cassano, G.B., 1999. Distribution and characterization of [3H]mesulergine binding in human brain postmortem. Eur. Neuropsychopharmacol. 10 (1), 21–26.

Milak, M.S., Severance, A.J., Prabhakaran, J., Kumar, J.S., Majo, V.J., Ogden, R.T., Mann, J.J., Parsey, R.V., 2011. In vivo serotonin-sensitive binding of [11C]CUMI-101: a serotonin 1A receptor agonist positron emission tomography radiotracer. J. Cereb. Blood Flow Metab. 31 (1), 243–249.

Millan, M.J., Gobert, A., Lejeune, F., Dekeyne, A., Newman-Tancredi, A., Pasteau, V., Rivet, J.M., Cussac, D., 2003. The novel melatonin agonist agomelatine (S20098) is an antagonist at 5-hydroxytryptamine2C receptors, blockade of which enhances the activity of frontocortical dopaminergic and adrenergic pathways. J. Pharmacol. Exp. Ther. 306 (3), 954–964.

Narendran, R., Hwang, D.R., Slifstein, M., Talbot, P.S., Erritzoe, D., Huang, Y., Cooper, T.B., Martinez, D., Kegeles, L.S., Abi-Dargham, A., Laruelle, M., 2004. In vivo vulnerability to competition by endogenous dopamine: comparison of the D2 receptor agonist radiotracer (−)-N-[11C]propyl-norapomorphine ([11C]NPA) with the D2 receptor antagonist radiotracer [11C]-raclopride. Synapse 52 (3), 188–208.

Narendran, R., Mason, N.S., Laymon, C.M., Lopresti, B.J., Velasquez, N.D., May, M.A., Kendro, S., Martinez, D., Mathis, C.A., Frankle, W.G., 2010. A comparative evaluation of the dopamine D(2/3) agonist radiotracer [11C](−)-N-propyl-norapomorphine and antagonist [11C]raclopride to measure amphetamine-induced dopamine release in the human striatum. J. Pharmacol. Exp. Ther. 333 (2), 533–539.

Nord, M., Finnema, S.J., Halldin, C., Farde, L., 2013. Effect of a single dose of escitalopram on serotonin concentration in the non-human and human primate brain. Int. J. Neuropsychopharmacol. 1–10.

Parker, C.A., Gunn, R.N., Rabiner, E.A., Slifstein, M., Comley, R., Salinas, C., Johnson, C.N., Jakobsen, S., Houle, S., Laruelle, M., Cunningham, V.J., Martarello, L., 2012. Radiosynthesis and characterization of 11C-GSK215083 as a PET radioligand for the 5-HT6 receptor. J. Nucl. Med. 53 (2), 295–303.

Paterson, L.M., Kornum, B.R., Nutt, D.J., Pike, V.W., Knudsen, G.M., 2013. 5-HT radioligands for human brain imaging with PET and SPECT. Med. Res. Rev. 33 (1), 54–111.

Pinborg, L.H., Adams, K.H., Svarer, C., Holm, S., Hasselbalch, S.G., Haugbol, S., Madsen, J., Knudsen, G.M., 2003. Quantification of 5-HT2A receptors in the human brain using [^{18}F]altanserin-PET and the bolus/infusion approach. J. Cereb. Blood Flow Metab. 23 (8), 985–996.

Pinborg, L.H., Adams, K.H., Yndgaard, S., Hasselbalch, S.G., Holm, S., Kristiansen, H., Paulson, O.B., Knudsen, G.M., 2004. [18F]altanserin binding to human 5HT2A receptors is unaltered after citalopram and pindolol challenge. J. Cereb. Blood Flow Metab. 24 (9), 1037–1045.

Quednow, B.B., Treyer, V., Hasler, F., Dorig, N., Wyss, M.T., Burger, C., Rentsch, K.M., Westera, G., Schubiger, P.A., Buck, A., Vollenweider, F.X., 2012. Assessment of serotonin release capacity in the human brain using dexfenfluramine challenge and [18F] altanserin positron emission tomography. NeuroImage 59 (4), 3922–3932.

Saleem, K.S., Logothesis, N.K., 2007. A combined MRI and Histology Atlas of the Rhesus Monkey Brain in Stereotaxic Coordinates. Academic Press, Oxford, U.K.

Selvaraj, S., Turkheimer, F., Rosso, L., Faulkner, P., Mouchlianitis, E., Roiser, J.P., McGuire, P., Cowen, P.J., Howes, O., 2012. Measuring endogenous changes in serotonergic neurotransmission in humans: a [11C]CUMI-101 PET challenge study. Mol. Psychiatry 17 (12), 1254–1260.

Seneca, N., Finnema, S.J., Farde, L., Gulyas, B., Wikstrom, H.V., Halldin, C., Innis, R.B., 2006. Effect of amphetamine on dopamine D2 receptor binding in nonhuman primate brain: a comparison of the agonist radioligand [11C]MNPA and antagonist [11C] raclopride. Synapse 59 (5), 260–269.

Shotbolt, P., Tziortzi, A.C., Searle, G.E., Colasanti, A., van der Aart, J., Abanades, S., Plisson, C., Miller, S.R., Huiban, M., Beaver, J.D., Gunn, R.N., Laruelle, M., Rabiner, E.A., 2012. Within-subject comparison of [(11)C]-(+)-PHNO and [(11)C]raclopride sensitivity to acute amphetamine challenge in healthy humans. J. Cereb. Blood Flow Metab. 32 (1), 127–136.

Slifstein, M., Parsey, R.V., Laruelle, M., 2000. Derivation of [(11)C]WAY-100635 binding parameters with reference tissue models: effect of violations of model assumptions. Nucl. Med. Biol. 27 (5), 487–492.

Smith, B.M., Smith, J.M., Tsai, J.H., Schultz, J.A., Gilson, C.A., Estrada, S.A., Chen, R.R., Park, D.M., Prieto, E.B., Gallardo, C.S., Sengupta, D., Dosa, P.I., Covel, J.A., Ren, A., Webb, R.R., Beeley, N.R., Martin, M., Morgan, M., Espitia, S., Saldana, H.R., Bjenning, C., Whelan, K.T., Grottick, A.J., Menzaghi, F., Thomsen, W.J., 2008. Discovery and structure-activity relationship of (1R)-8-chloro-2,3,4,5-tetrahydro-1-methyl-1H-3-benzazepine (lorcaserin), a selective serotonin 5-HT2C receptor agonist for the treatment of obesity. J. Med. Chem. 51 (2), 305–313.

Song, J., Hanniford, D., Doucette, C., Graham, E., Poole, M.F., Ting, A., Sherf, B., Harrington, J., Brunden, K., Stricker-Krongrad, A., 2005. Development of homogeneous high-affinity agonist binding assays for 5-HT2 receptor subtypes. Assay Drug Dev. Technol. 3 (6), 649–659.

Staley, J.K., Van Dyck, C.H., Tan, P.Z., Al Tikriti, M., Ramsby, Q., Klump, H., Ng, C., Garg, P., Soufer, R., Baldwin, R.M., Innis, R.B., 2001. Comparison of [(18)F]altanserin and [(18)F]deuteroaltanserin for PET imaging of serotonin(2A) receptors in baboon brain: pharmacological studies. Nucl. Med. Biol. 28 (3), 271–279.

Talbot, P.S., Slifstein, M., Hwang, D.R., Huang, Y., Scher, E., Abi-Dargham, A., Laruelle, M., 2012. Extended characterisation of the serotonin 2A (5-HT2A) receptor-selective PET radiotracer 11C-MDL100907 in humans: quantitative analysis, test-retest reproducibility, and vulnerability to endogenous 5-HT tone. NeuroImage 59 (1), 271–285.

Thomsen, W.J., Grottick, A.J., Menzaghi, F., Reyes-Saldana, H., Espitia, S., Yuskin, D., Whelan, K., Martin, M., Morgan, M., Chen, W., Al-Shamma, H., Smith, B., Chalmers, D., Behan, D., 2008. Lorcaserin, a novel selective human 5-hydroxytryptamine2C agonist: in vitro and in vivo pharmacological characterization. J. Pharmacol. Exp. Ther. 325 (2), 577–587.

Varrone, A., Sjoholm, N., Eriksson, L., Gulyas, B., Halldin, C., Farde, L., 2009. Advancement in PET quantification using 3D-OP-OSEM point spread function reconstruction with the HRRT. Eur. J. Nucl. Med. Mol. Imaging 36 (10), 1639–1650.